World Academy of Science, Engineering and Technology
International Journal of Mechanical and Mechatronics Engineering
Vol:11, No:8, 2017

# Parametric Analysis of Solid Oxide Fuel Cell Using Lattice Boltzmann Method

Abir Yahya, Hacen Dhahri, Khalifa Slimi



***Abstract*—**The present paper deals with a numerical simulation of temperature field inside a solid oxide fuel cell (SOFC) components. The temperature distribution is investigated using a co-flow planar SOFC comprising the air and fuel channel and two-ceramic electrodes, anode and cathode, separated by a dense ceramic electrolyte. The Lattice Boltzmann method (LBM) is used for the numerical simulation of the physical problem. The effects of inlet temperature, anode thermal conductivity and current density on temperature distribution are discussed. It was found that temperature distribution is very sensitive to the inlet temperature and the current density.

***Keywords*—**Solid oxide fuel cell, Heat sources, temperature, Lattice Boltzmann method.

## I. Introduction

THE SOFC has drawn attention because of its higher energy conversion efficiency, power density, low environmental hazards and production cost [1], [2]. Currently, most of the studies on SOFCs are focused on the development of novel electrolyte materials or electrochemically active catalysts. For comparison, mathematical modeling is much more time-efficient and economically sound to understand the physical/chemical phenomena involved in SOFC operation. Parametric analysis was conducted to study the effects of operating parameters on SOFC performance [3]. Arpino et al. [4] have developed a numerical model to simulate energy and mass transport phenomena in SOFCs. Thinh et al. [5] presented the results of temperature, chemical species and current density distribution of a planar anode -supported SOFC for both co- and counter-flow configurations. The LBM is a powerful numerical technique based on kinetic theory for simulating fluid flows and modeling the physics in fluids [6], [7]. LBM has shown promising simulation results of fluid flows and mass diffusion through complex geometries and this is an attractive characteristic for fuel cell modeling.

In this paper, the temperature distribution was investigated using a single computational domain comprising the air and fuel channel and the electrolyte-electrodes assembly. The governing equations for momentum and energy conservation were discretized with the LBM.

The main objective of this work is to analyze the effects of heat sources on temperature field inside SOFC components. Special attention will be paid to examine the effects of operating parameters such as inlet temperature, anode thermal conductivity and current density on distribution of temperature inside the SOFC.

Abir Yahya is with the National Engineering School of Monastir, Tunisia (e-mail: yahyaabir486@yahoo.com).

## II. Physical Model

The SOFC is divided into three computational domains; the anodic and cathodic compartments, which consists of flow channel and electrodes, and the electrolyte domain. Hydrogen and air are introduced in the anode and cathode, respectively (Fig. 1).

At the cathode, oxygen molecules diffuse to the cathode-electrolyte interface where they are reduced to oxygen ions with the help of the electrons. Further, the oxygen ions migrate through the dense ion conducting electrolyte to the anode-electrolyte interface. At the anode, hydrogen gas molecules transport through the porous anode to the anode-electrolyte interface where they react with oxygen ions to produce water. At the same time, the releasing electrons are transported to the cathode via an external circuit, resulting in electrical power [4].

The electrochemical reactions that take place at the anode and cathode are as follows:

Anode: $H_2 + O^{2-} \rightarrow H_2O + 2e^-$

Cathode: $\frac{1}{2}O_2 + 2e^- \rightarrow O^{2-}$

Based on these half-cell reactions, the net reaction can be written as:

$$H_2 + \frac{1}{2}O_2 \rightarrow H_2O$$

It is worth noting that the following assumptions are considered:

- The flow is incompressible;
- The fluids can be described by using the ideal gas law;
- Thermodynamic properties of the media are constant; and,
- No electro-chemical reactions occur in the air and the fuel channels.

TABLE I
Geometry Parameters of the Planar SOFC

| Component | Value |
|---|---|
| Anode thickness | 500 μm |
| Electrolyte thickness | 10 μm |
| Cathode thickness | 50 μm |
| Anode channel height | 2.5 mm |
| Cathode channel width | 2.5 mm |
| Anode channel width | 2.5 mm |
| Cathode channel height | 500 μm |
| Cell length | 100 mm |

The detailed geometric parameters and operation conditions

for the simulation in the work are listed in Tables I and II, respectively [8].

TABLE II
CONDITIONS AND PARAMETERS FOR SIMULATION

| Parameter | Value |
|---|---|
| Fuel inlet composition (molar fraction) | 97% $H_2$ +3% $H_2O$ |
| Oxidant inlet composition(molar fraction) | 21% $O_2$ +79 % $N_2$ |
| Fuel inlet temperature, K | 800 |
| Oxidant inlet temperature, K | 800 |
| Cathode flow channel (air), $Nm^3s^{-1}$ | 4.4 $10^{-7}$ |
| anode flow channel (fuel), $Nm^3s^{-1}$ | 7.9 $10^{-7}$ |
| Air dynamic viscosity, $m^2s^{-1}$ | 2.3 $10^{-5}$ |
| Anode porosity | 0.3 |
| Cathode porosity | 0.3 |
| Thermal conductivity of anode Ni-YSZ ($Wm^{-1}$ $K^{-1}$) | 2 |
| Thermal conductivity of cathode LSM ($Wm^{-1}$ $K^{-1}$) | 2 |
| Thermal conductivity of electrolyte YSZ ($Wm^{-1}$ $K^{-1}$ | 2 |
| Electric resistivity of anode (Ωm) | 2.89 $10^{-5}$ exp (-1392/T) |
| Electric resistivity of cathode (Ωm) | 8.11 $10^{-5}$ exp (600/T) |
| Ionic resistivity of electrolyte (Ωm) | 2.94 $10^{-5}$ exp (1010350/T) |
| α (V) | 0.04 |
| β (V) | 0.002 |
| Jn ($mA/cm^2$) | 2 |
| J0 ($mA/cm^2$) | 0.02 |
| J1 ($mA/cm^2$) | 670 |

## III. MATHEMATICAL MODEL

The heat transfer phenomena in an SOFC are governed by the conservation laws of momentum and energy.

### A. Continuity Equation

$$\frac{\partial(\rho U)}{\partial x}+\frac{\partial(\rho V)}{\partial y}=0 \quad (1)$$

### B. Momentum Equation

To model the flow field profile in the channels and the porous electrodes, the general Navier-Stokes equation was employed [9].

$$\frac{\partial(\rho U)}{\partial t}+\frac{\partial(\rho UU)}{\partial x}+\frac{\partial(\rho VU)}{\partial y}=-\frac{\partial(P)}{\partial x}+\frac{\partial}{\partial x}\left(\mu\frac{\partial U}{\partial x}\right)+\frac{\partial}{\partial y}\left(\mu\frac{\partial U}{\partial y}\right)+S_x \quad (2)$$

$$\frac{\partial(\rho V)}{\partial t}+\frac{\partial(\rho UV)}{\partial x}+\frac{\partial(\rho VV)}{\partial y}=-\frac{\partial(P)}{\partial x}+\frac{\partial}{\partial x}\left(\mu\frac{\partial V}{\partial x}\right)+\frac{\partial}{\partial y}\left(\mu\frac{\partial V}{\partial y}\right)+S_y \quad (3)$$

The source terms Sx and Sy are determined by Darcy's law for both anode and cathode

$$S_x=-\frac{\mu}{k}\varepsilon U \quad (4)$$

$$S_y=-\frac{\mu}{k}\varepsilon V \quad (5)$$

where k is the permeability of the porous electrodes, ρ is the density, ε is the porosity and μ is the dynamic viscosity.

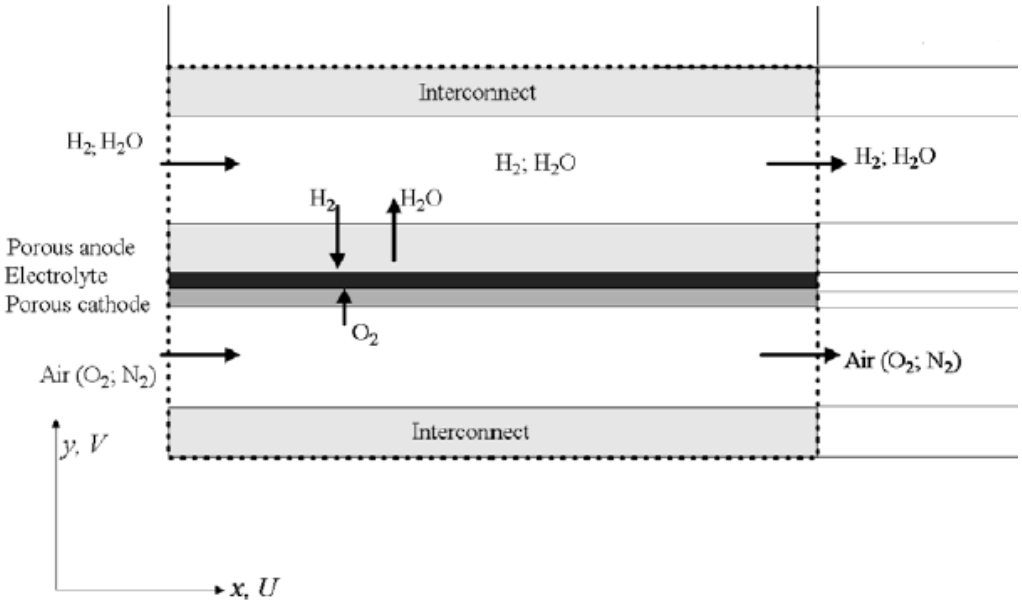


Fig. 1 Schematic representation of a planar SOFC

### C. Energy Equation

The dominating phenomena in this model are heat convection and heat conduction, while the radiative heat transfer is assumed to be negligible.

$$\frac{\partial\left[(\rho c_p)_{eff}T\right]}{\partial t}+\frac{\partial\left[(\rho c_p)_{eff}UT\right]}{\partial x}+\frac{\partial\left[(\rho c_p)_{eff}VT\right]}{\partial y}=\frac{\partial}{\partial x}\left(\lambda_{eff}\frac{\partial T}{\partial x}\right)+\frac{\partial}{\partial y}\left(\lambda_{eff}\frac{\partial T}{\partial y}\right)+S_T \quad (6)$$

where $c_p$ is the specific heat capacity, and λ is the thermal

conductivity. The subscripts eff mean effective. $S_T$ is the heat source term resulting from the Joule heating, activation polarization heat and chemical reaction heat [10].

- **Joule Heating**

Like any other conductors, the electrodes produce a resistance to the electrons, and the electrolyte has a resistance to the ions. The losses associated with these resistances is called Joule heating and it is expressed as [11]:

$$S_J = \sum R_{ohm} j^2 \quad (7)$$

- **Chemical Reaction Heat**

The heat generated by the electrochemical reactions can be evaluated by electrical work and enthalpy changes. The electrochemical heat is thermal energy released at the anode-electrolyte interface and determined as [12]:

$$S_r = \frac{T\Delta S}{2F} j \quad (8)$$

where ΔS is the entropy expressed as [13].

$$\Delta S = \Delta S_0 + \int_{298}^{T} \frac{\Delta C_{pr}}{T} dT \quad (9)$$

with:

$$C_{pr} = C_{pH_2O} - C_{pH_2} - 0.5\, C_{pO_2} \quad (10)$$

The water, hydrogen, oxygen specific heats vs. temperature are expressed by the following expression [10].

$$C_p = \sum a_i \left(\frac{T}{1000}\right)^i \ (i = 1,6) \quad (11)$$

where ai are coefficients for $H_2$, $H_2O$ and $O_2$.

- **Activation Polarization Heat**

The Tafel equation [10] provides a general equation giving the values of activation losses in the anode and the cathode, as:

$$S_{act} = j\left[\alpha \ln\left(\frac{j+j_n}{j_0}\right)\right] \quad (12)$$

*D. Boundary Conditions*

At the entrance region (i.e. at x=0), a constant flow velocity U=Uin is specified of the gas flow channels, while U=0 is specified for the solid part. Similarly, a constant temperature is specified at the inlet for both the gas flow channels and the solid part. At both bottom and top walls of the computation zone (i.e. at y=0 and y=yM), thermally adiabatic conditions are assumed: ∂T/∂y=0. At the outlet of the computation domain (i.e. at x=xL), the gas flow channels we have ∂U/∂x= 0 and ∂T/∂x=0, while for the solid part, U=0, V=0 and ∂T/∂x=0 are employed.

## IV. Numerical Method

The LBM has been successfully applied to fluid dynamics and heat transfer problems including fluid flows in porous media, thermal two-phase flow and diffusion in multi component fluids [14].

In this work the D2Q9 model, which consists of nine distribution functions, has been used. The developed Lattice Boltzmann equation (LBE) of a density distribution function for the evolution of the velocity field is given as [15]:

$$f_i(x + e_i\,\Delta t, t + \Delta t) - f_i(x,t) = -\frac{1}{\tau}\left[f_i(x,t) - f_i^{eq}(x,t)\right] + \Delta t F_i \quad (13)$$

The equilibrium distribution function is expressed as:

$$f_i^{eq}(x,t) = w_i \rho \left[1 + \frac{e_i u}{c_s^2} + \frac{(e_i u)^2}{2\varepsilon c_s^4} - \frac{u^2}{2\varepsilon c_s^2}\right] \quad (14)$$

where wi is the weighting factor and ρ is the lattice fluid density. For the D2Q9 model, the values of ei and wi have special values for various i directions.

$$w_0 = \frac{4}{9}, w_{1-4} = \frac{1}{9}, w_{5-9} = \frac{1}{36} \quad (15)$$

$$e_i = \begin{Bmatrix} 0 \ i = 0 \\ c\left(\cos\frac{(i-1)\pi}{2}, \sin\frac{(i-1)\pi}{2}\right) \ i = 1,2,3,4 \\ \sqrt{2}\, c\left(\cos\left[\frac{(i-5)\pi}{2} + \frac{\pi}{4}\right], \sin\left[\frac{(i-1)\pi}{2} + \frac{\pi}{4}\right]\right) \ i = 5,6,7,8 \end{Bmatrix} \quad (16)$$

After evolving on the discrete lattices, the density and velocity can be calculated using

$$\rho = \sum_i f_i \quad (17)$$

$$\rho u = \sum_i e_i f_i \quad (18)$$

Based on the work of Jinku Wang [16], the evolution equation for heat transfer can be generally given as:

$$g_i(x + e_i\,\Delta t, t + \Delta t) - g_i(x,t) = -\frac{1}{\tau_g}\left[g_i(x,t) - g_i^{eq}(x,t)\right] + \Delta t G_i \quad (19)$$

where the equilibrium distribution is

$$g_i^{eq}(x,t) = w_i T\left[1 + \frac{e_i u}{c_s^2}\right] \quad (20)$$

Jinku Wang proposed an expression for the forcing term $S_T$ appearing in the energy equation:

$$G_i = w_i\left(1 - \frac{0.5}{\tau_g}\right)\frac{S_T}{\rho c_p} \quad (21)$$

The temperature can be calculated from the following equation:

$$T = \sum_i g_i + \frac{\Delta t}{2}\frac{S_T}{\rho c_p} \quad (22)$$

Boundary conditions are very important and crucial for the accuracy and stability of LBM simulation. For the inlet boundary, known velocity and temperature Zou and He condition [17] is used. As for outlet, the open boundary is

applied and for adiabatic walls, the condition of Bounce Back is applied [18].

## V. Results and Discussion

### A. Model Validation

The present numerical code was validated with the published study of Mahecene et al. [8], where they have used a single-unit model with double channel of co-flow pattern, the inlet temperature at the hydrogen and air channels is TH2 = Tair = 800 K and the cell current density is 10 000 A/m2.

Fig. 2 depicts a comparison between our results and those of Mahecene et al. As it can be seen from this figure, a satisfactory agreement between our results and those reported in the literature. Fig. 2 illustrates the temperature distribution in the presence of the heat sources effect: Figs. 2 (a) and (d) activation losses, Figs. 2 (b) and (e) ohmic losses, and Figs. 2 (c) and (f) chemical reaction. The activation over potential heat source type is related to the electron transfer reactions at the electrodes. This type of heat source creates an important heat quantity which influences in the temperature until achieved a value T= 994.75 K. The effect of the heat source due to the ohmic over potentials is remarkable for the gaseous temperature T= 800K. The maximum temperature value is 1001.8 K.

The heat source, due to the chemical reaction, is released in the interface of the anode and electrolyte, from these hot sites, heat is transmitted to the other parts of the cell. Chemical reactions creates the lowest heat source, the maximum temperature value is 984.69 K.

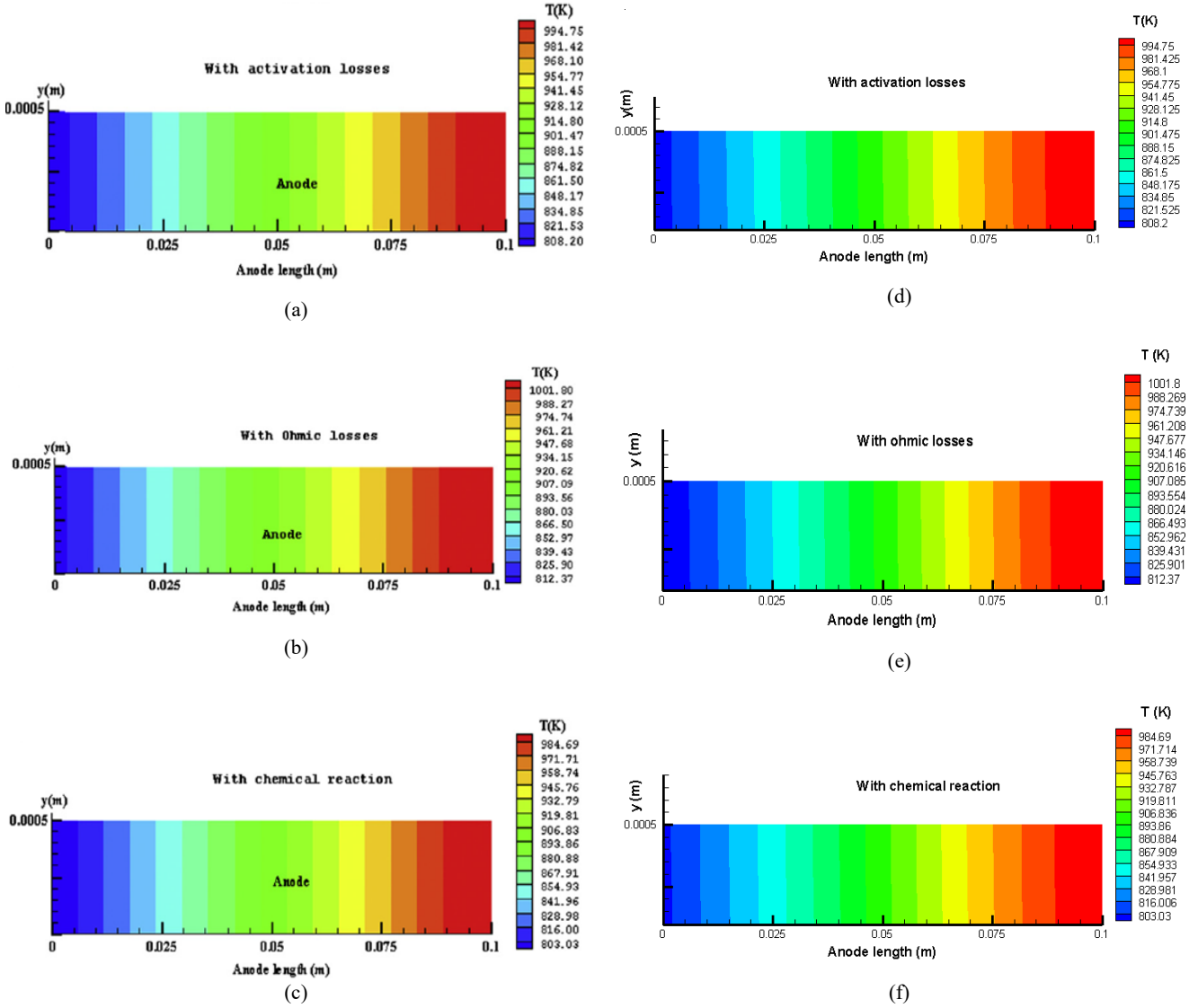


Fig. 2 Comparison of temperature distribution at the anode between present study and Mahecene et al. [8]; (a)-(c) present study, (d)-(f) Mahecene et al., (a), (d) activation losses, (b), (e) ohmic losses and (c), (f) chemical reaction losses

*B. Effect of the Operating Temperature*

Fig. 3 describes the effect of the inlet temperature on anode temperature profiles. The temperature difference in presence of ohmic losses rises with the increase of the operating temperature because the ionic resistivity of the electrolyte and electric resistivity of electrodes are very sensitive to the temperature. Similarly, the presence of activation losses presents the same trend as that of ohmic losses because a higher inlet temperature leads to more reactive electrodes. Referring to Fig. 3 (c), the temperature difference in presence of chemical reaction losses gets higher with increasing the temperature because the water, hydrogen and oxygen specific heats are expressed according to the temperature.

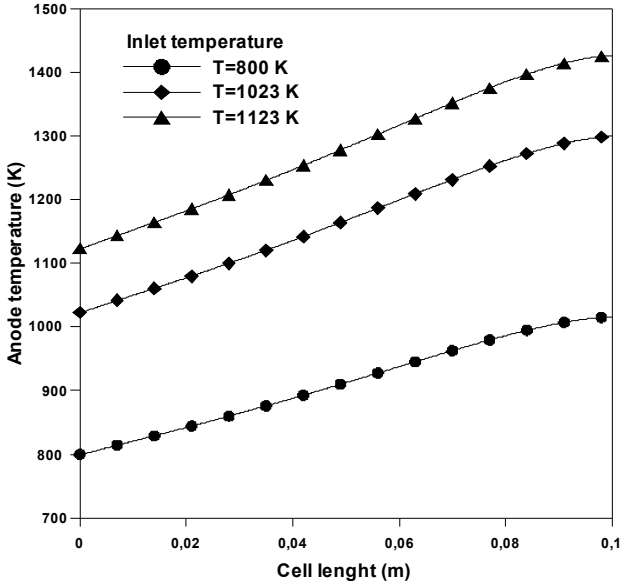


(a)

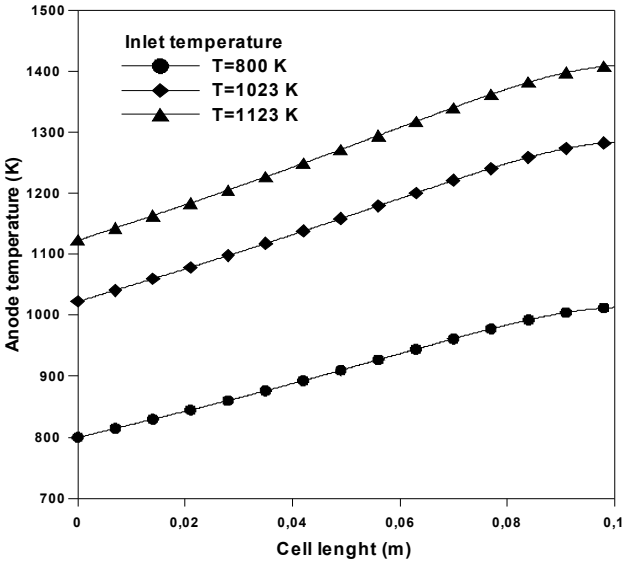


(b)

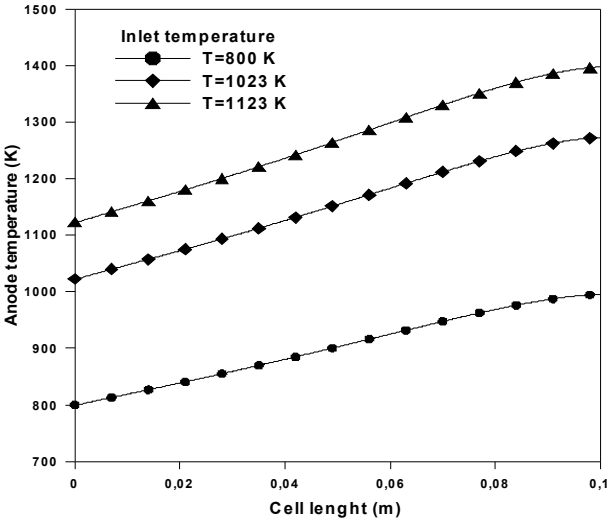


(c)

Fig. 3 Effect of operating temperature at j=10 000 A/m2; (a) temperature with ohmic losses, (b) temperature with activation losses and (c) temperature with chemical reaction losses

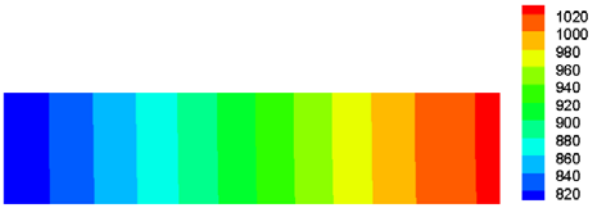


(a)

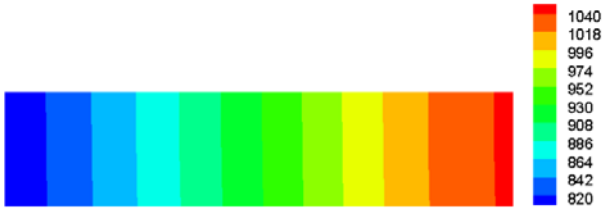


(b)

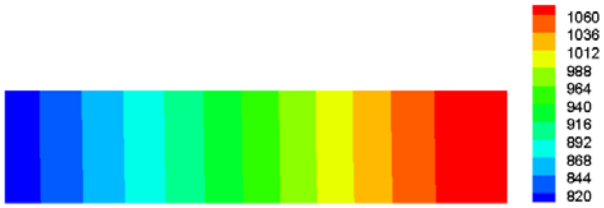


(c)

Fig. 4 Temperature distribution of anode at different current density at T=800K; (a) j=10 000 A/m$^2$, (b) j=15 000 A/m$^2$ and (d) j=20 000 A/m$^2$

*C. Effect of the Current Density*

The increase in temperature of SOFC is the result of heat generation due to chemical reactions, joule and activation losses, which depend on the current density.

The effects of current density on the temperature

distribution are shown in Fig. 4. As depicted from this figure, the temperature increases with the increase of the current density which is attributed to relativity higher heat generation at higher currents due to both enhanced electrochemical reactions and joule heating.

*D. Effect of Anode Thermal Conductivity*

The thermal properties of the anode Ni/YSZ are very sensitive to the composition and porosity. The thermal conductivity of the cermet became larger as the Ni concentration increased. Moreover, whatever the composition, the thermal conductivity of the cermet varied linearly with respect to the temperature. Concerning the porosity dependence of the thermal conductivity of Ni/YSZ cermets, a remarkable decrease in the thermal conductivity with an increased porosity could be observed, which indicates that the pores in the cermet are thermal barriers against heat transfer [19].

Fig. 5 shows the temperature distribution for various thermal conductivities of porous Ni/YSZ cermets. By comparing, it is found that there is a similar trend for the temperature profiles. The temperature increases along the direction of fuel flow. For the case of high thermal conductivity, the maximum temperature 1220 K is bigger compare to that of low thermal conductivity 1023 K.

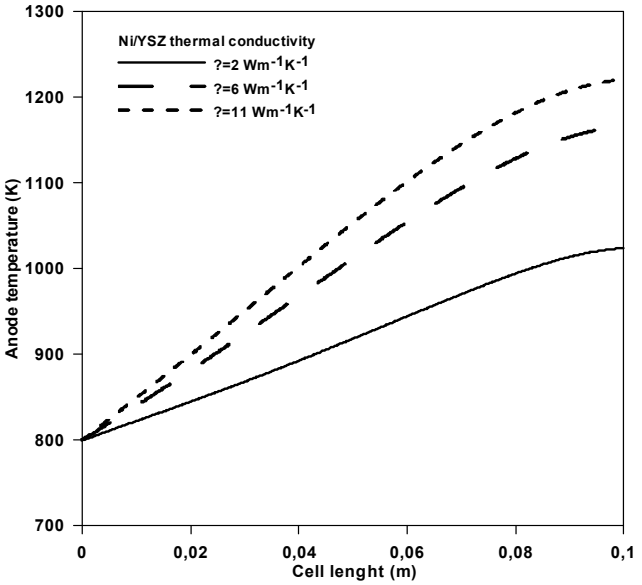


Fig. 5 Temperature profiles for various thermal conductivities of porous Ni/YSZ

*E. Heat Transfer Rate*

The heat transfer is commonly used to express the rate at which heat can be advected from a surface. The Nusselt number is defined in the context of channel flow as:

$$Nu = \frac{\left(\frac{\partial T}{\partial y}\right)_s}{(T_{bulk} - T_s)/H} \quad (23)$$

where $\left(\frac{\partial T}{\partial y}\right)_s$ is the temperature gradient at surface and $(T_{bulk} - T_s)/H$ is the overall temperature gradient.

The variation of Nusselt number along the axial coordinate in the SOFC, in the presence of different heat losses, is explored in Fig. 6. As shown, the Nusselt number is relatively high near the inlet but decays rapidly to a rather uniform value after short distance of about 1 cm, due to the thermal boundary-layer development. It can also be noticed that the Nusselt number decreases again along the main stream direction at the exit of the duct which is caused by the changing heat flux. Slightly higher Nusselt number in the air channel is believed to be caused by the suction effect due to oxygen consumption in the cathode.

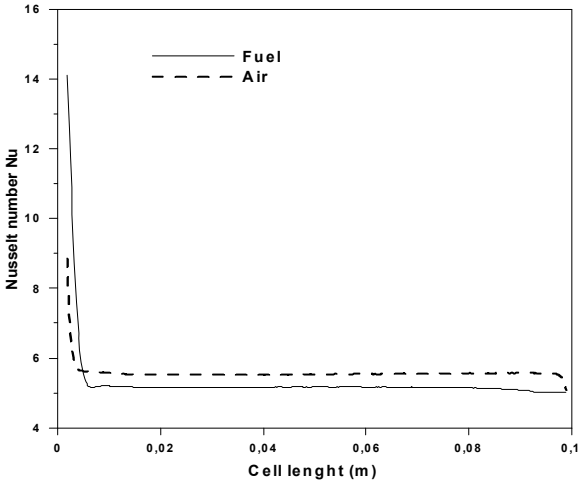


(a)

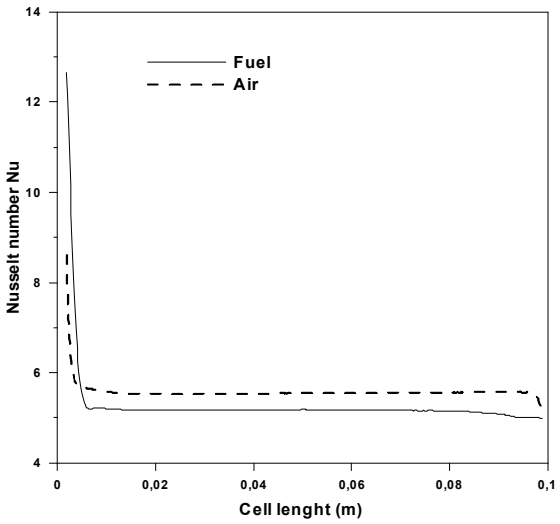


(b)

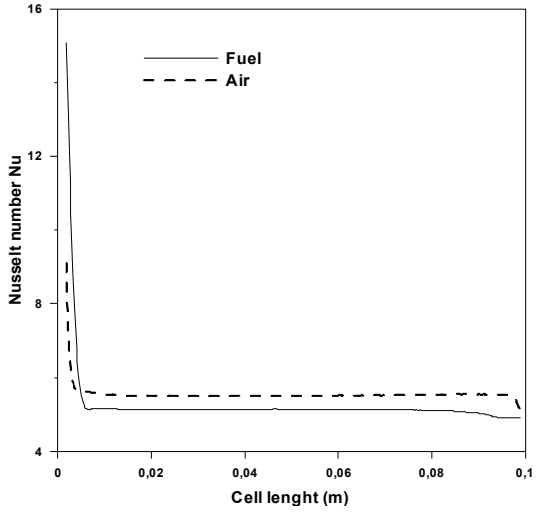


(c)

Fig. 6 Variation of Nusselt number along the axial coordinate in SOFC at T=800 K and j=10 000 A/m$^2$ with the presence of: (a) ohmic losses, (b) activation losses and (c) chemical reaction losses

## VI. Conclusion

A planar SOFC has been investigated numerically. The present work focuses on the effects of various heat sources on temperature distribution of SOFC components (channels cathode, anode and electrolyte).

Parametric analyses were performed to determinate the effects of geometrical and operating parameters on the temperature distribution.

## Nomenclature

| Symbol | Quantity |
|---|---|
| Cp | Heat capacity (JKg$^{-1}$K$^{-1}$) |
| Cs | Speed of sound (ms$^{-1}$) |
| e | Discrete lattice velocity in direction i (ms$^{-1}$) |
| F | Faraday constant (96484.56 C mol$^{-1}$) |
| $F_i$ | Discrete body force (kgm$^{-3}$ s$^{-1}$) |
| $f_i$ | Density distribution function |
| $f_i^{eq}$ | Equilibrium distribution function for fi |
| $g_i$ | Energy distribution function |
| $g_i^{eq}$ | Equilibrium distribution function for gi |
| $G_i$ | Discrete body force of energy |
| $h_t$ | Convective heat transfer coefficient |
| ΔS | Entropy (J mol$^{-1}$ K$^{-1}$) |
| j | Total current density (A m$^{-2}$) |
| k | Permeability (m$^2$ ) |
| P | Operating pressure (bar) |
| Rohm | Electric resistivity (Ωm) |
| ST | Heat source (Wm-3) |
| Sj | Joule heat source (Wm-3) |
| Sr | Chemical reaction heat source (Wm-3) |
| Sact | Activation heat source (Wm-3) |
| Sx,Sy | Source term |
| T | Temperature (K) |
| u | Velocity vector (ms-1) |
| U,V | Local velocity (m s-1) |
| Ɛ | Porosity |
| ρ | Density (Kg m-3) |
| μ | Dynamic viscosity (Kg m-1s-1 ) |
| λ | Thermal conductivity (Wm-1K-1) |
| τ | Relaxation time for fi |

## References

[1] Singhal SC. Advances in solid oxide fuel cell technology. Solid State Ionics 135 (2000) 305–313.
[2] Singhal SC. Solid oxide fuel cells for stationary, mobile, and military applications. Solid State Ionics 152–153 (2002) 405–410.
[3] Ni M.2D thermal-fluid modeling and parametric analysis of a planar solid oxide fuel cell, Energy conversion and Management 51 (2010) 714-721.
[4] Arpino F, Massarotti N. Numerical simulation of mass and energy transport phenomena in solid oxide fuel cells. Energy 34 (2009) 2033-2041.
[5] Ho TX, Kosinski P, Hoffmann AC, Vik A. Effects of heat sources on the performance of a planar solid oxide fuel cell. International Journal of Hydrogen Energy 35 (2010) 4276-4284.
[6] Chen S, Doolen GD. Lattice Boltzmann method for fluid flows. Annu Rev Fluid Mech 30 (1998) 329-64.
[7] Mohammad AA. Applied lattice Boltzmann method for transport phenomena momentum heat and mass transfer. The university of Calgary Press;2007.
[8] Mahecene H, Ben moussa H, Bouguettaia H, Bechki D, Babay S, Meftah MS. Study of species, temperature distributions and the solid oxide fuel cells performance in a 2-D model. International journal Of Hydrogen Energy 36 (2011) 4244-4252.
[9] Chaisantikulwat. A, Diaz-Goano. C, Meadows. E. S. Dynamic modelling and control of planar anode-supported solid oxide fuel cell. Computres & Chemical Engineering 2008;32:2365-2381.
[10] Yixin L. Numerical simulation of a flat-tube high power density solid oxide fuel cell. PhD thesis (2005). University of Pittsburgh.
[11] Ramirez-Minguela. J. J, Rodriguez-Munoz. J. L, Perez-Garcia. V, Mendoza-Miranda. J. M, Munoz-Carpio. V. D, Alfaro-Ayala. J. A. Solid oxde fuel cell numerical study: modified MOLB-type and simple planar geometries with internal reforming. Electrochimica Acta 2015;159:149-157.
[12] Zitouni B, Ben Moussa H, Oulmi K, Saighi S, Chetehouna K. Temperature field, H2 and H2O mass transfer in SOFC single cell: Electrode and electrolyte thickness effects. International Journal of Hydrogen Energy 2009; 34:5032-5039
[13] Mandin P, Bernay C, Tran-Dac S, Broto A, Abes D, Cassir M. SOFC modelling and numerical simulation of performance. J Fuel Cells 2006;6(1):71–8.
[14] Guo Z, Zhao TS, Lattice Boltzmann simulation of natural convection with temperature dependent viscosity in a porous cavity, Journal of Progress in Computational Fluid Dynamics 2005;5:110-117.
[15] Bai H, Yu P., Winoto H, Low HT. Lattice Boltzmann method for flows in porous and homogenous fluid domains coupled at the interface by stress jump. International Journal for Numerical Methods in Fluids 2009;60:691-708.
[16] Wang J, Wang M, Li Z. A lattice Boltzmann algorithm for fluid-solid conjugate heat transfer. International Journal of Thermal Sciences 2007;46:228-234.
[17] Zou. Q, He. X. On pressure and velocity boundary conditions for the lattice Boltzmann BGK model, Physics of Fluids,1997;6: 1591-1598.
[18] Mohamad, A., Lattice Boltzmann method fundamentals and engineering applications with computer codes, Dept. of mechanical and manufacturing engineering, Schulich School of Engineering, the University of Calgary, Alberta, Canada, ISBN 978-0-9783253-0-5, 2-31, 2011.
[19] T. Kawashima, M. Hishinuma, Thermal Properties of porous Ni/YSZ particulate composites at high temperatures, Mater. Trans. JIM 37 (9) (1996) 1518–1524.